Pergamon

Geochimica et Cosmochimica Acta, Vol. 60, No. 12, pp. 2153–2166, 1996

0016-7037/96 $15.00 + .00

PII S0016-7037(96)00078-6

MORB mantle and subduction components interact to generate basalts in the southern Mariana Trough back-arc basin

ROBERT F. GRIBBLE,[1] ROBERT J. STERN,[1] SHERMAN H. BLOOMER,[2] DORIS STÜBEN,[3] TIM O'HEARN,[4] and SALLY NEWMAN[5]

[1]Center for Lithospheric Studies, University of Texas at Dallas, Richardson, TX 75083-0688, USA
[2]Department of Geosciences, Oregon State University, Corvallis, OR 97331, USA
[3]Institute of Petrography and Geochemistry, University of Karlsruhe, D-76128 Karlsruhe, Germany
[4]Smithsonian Institution, Washington, DC 20560, USA
[5]Division of Geological and Planetary Science, California Institute of Technology, Pasadena, CA 91125, USA

(*Received March* 15, 1995; *accepted in revised form February* 26, 1996)

Abstract—We report the results of the first geochemical and isotopic survey of basaltic glasses dredged along the spreading ridge of the southern Mariana Trough (SMT; 15–17°N). This ridge is divided into two segments that have different axial depths, major and trace element compositions, water contents, and isotopic compositions of Sr, Nd, and Pb. Glasses from the shallower, northern segment (N-SMT; 16–17°N) are OL- and QZ-tholeiites that have compositions consistent with a higher degree of mantle melting relative to that of the OL tholeiites from the southern ridge segment (S-SMT; 15–16°N). The N-SMT glasses are similar to basalts erupted near 18°N in the Mariana Trough that have been the focus of previous studies. The more extensive melting inferred for the N-SMT correlates well with higher abundances of water and relative abundances of large ion lithophile and light Rare Earth elements that indicate involvement of a subduction component. The southern ridge segment is deeper and erupts compositions characteristic of lower degrees of melting; this correlates well with a lower proportion of the subduction component, including a suite that is indistinguishable from MORB. The strong correlation between degree of melting, water contents, and LIL elements indicates that hydrous fluxing as well as adiabatic decompression control melting of MORB-like mantle beneath back-arc basins. Details regarding the nature of this hydrous fluxing agent are not known, but it could be water-rich melts related to behind-the-arc volcanoes. These melts may be diverted by the back-arc convective regime, to become entrained in the zone of adiabatic upwelling, where they further stimulate melting.

1. INTRODUCTION

Basalts generated in back-arc basins, such as the Mariana Trough, provide valuable perspectives on mantle structure and composition, on controls for melt generation, and on the sources responsible for arc magma genesis. This is because back-arc basin basalts (BABB) are generated by decompression melting and erupt along spreading ridges in a manner indistinguishable from that of true MORB (Klein and Langmuir, 1987) and in most compositional aspects are similar to MORB. At the same time, a subduction component also is clearly involved (Hawkins et al., 1990), so BABB provide insights into modifications of the mantle at convergent margins (note that the term, subduction component, reflects the widely acknowledged compositional features unique to convergent margin magmas that are ultimately caused by water released from the subducted slab and involved in melt generation. Whether or not these unique compositional features reflect elements derived from the slab or stripped from the mantle is controversial; cf. Pearce and Peate, 1995).

There are three ways in which MORB and subduction components may interact: (1) magma (or source) mixing, (2) flux melting, and (3) assimilation. Magma mixing between MORB and arc magmas is predicted in young, narrow back-arc basins where arc and back-arc basin magma conduits may easily intersect (Stern et al., 1990). Flux melting may occur when subduction component fluids or melts infiltrate MORB mantle (Stolper and Newman, 1994). Finally, ascending melts may traverse and be contaminated by arc lithosphere that is stretched during the early stages of BAB formation or by rafts of arc lithosphere trapped in near-axial positions within mature BAB (Volpe et al., 1990).

Our objective is to infer the nature, source, and mode of introduction of materials that modify the proposed N-MORB mantle source of back-arc basin basalts. The study is based on an examination of fresh glasses collected along a portion of the Mariana Trough not previously sampled. We report major and trace element and radiogenic isotope data for basalts from the southern Mariana Trough (SMT) spreading axis between 17°30′N and 15°N and use these data to explore reasons for the continued influence of a 'subduction component' along a spreading axis within a relatively mature portion of a back-arc basin.

2. GEOLOGIC SETTING

The Mariana Trough is an actively spreading back-arc basin behind (west of) the Mariana arc (for an excellent review, see Fryer, 1995). The axis of spreading is not located in the middle of the Mariana Trough but is displaced toward the arc. The spreading axis is about 100 km west of the active arc at 18°N and only 50 km west of the arc at the latitude of Guam (Fig. 1). Bibee et al. (1980) concluded that seafloor spreading has been symmetrical over the last 3 Ma and that the present position of the ridge reflects a ridge jump, but Fryer (1995) argued that the western portion of the basin is underlain by mechanically extended lithosphere. The Benioff-Wadati zone dips beneath the arc but plunges vertically just west of the arc, so that the portion of the spreading axis sampled in this study (and at 18°N) is located 40 to 60 km west of the surface projection of the seismic zone's westernmost extent (Fig. 1 and Eguchi, 1984).

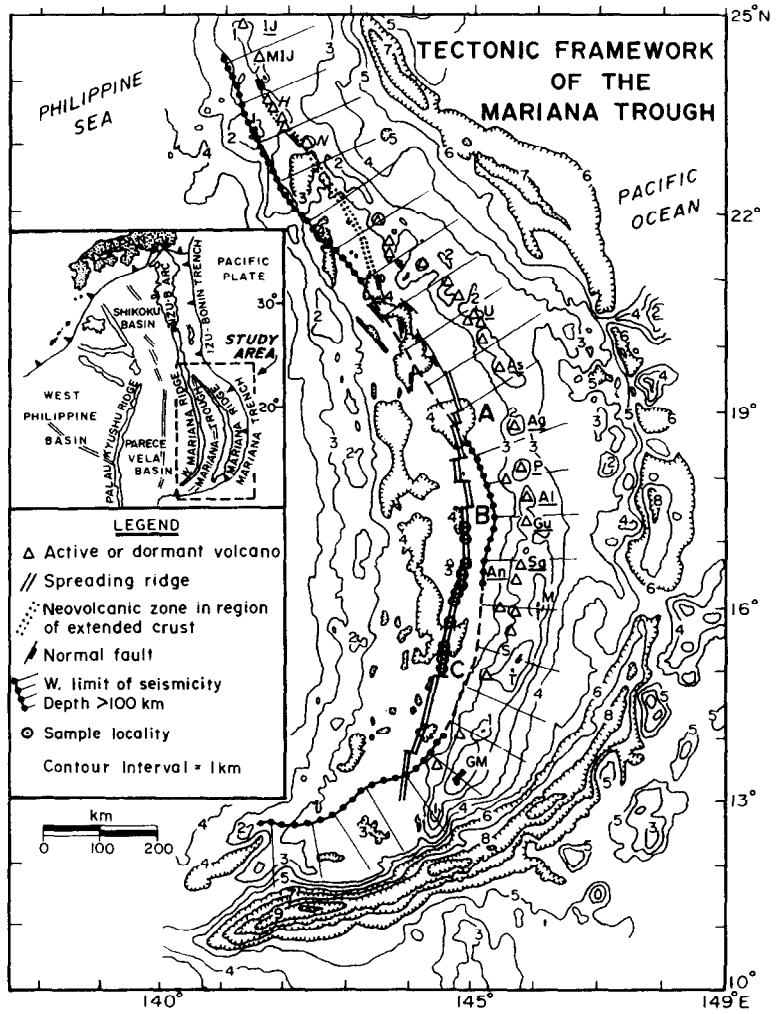

FIG. 1. Tectonic framework and location map of the Mariana arc system showing the extension axis of the Mariana Trough and sample localities (circled dots) of the R/V Sonne 69. A, B, and C mark the ridge section boundaries shown in Fig. 2. The hachured region is the surface projection of the westward extent of the Wadati-Beniof zone (Eguchi, 1984). Frontal arc islands of Guam (GM), Tinian (T), Saipan (S), and Medinilla (M) are shown. Open triangles denote position of arc volcanoes. (Plain = subaerial, italicized = submarine. Underlined are active or dormant: *An* = Anatahan; *Sa* = Sarigan; *Gu* = Guguan; *Al* = Alamagan; *P* = Pagan; *Ag* = Agrigan; *As* = Asuncion; *U* = Uracas; *IJ* = Iwo Jima. Not underlined are extinct: MIJ = Minami Iwo Jima. Submarine volcanoes include Nikko (*N*) and the Hiyoshi Volcanic Complex (*H*). Note that the boundary between the Central Island Province to the north and the Southern Seamount Province to the south lies just south of Anatahan, near 16°N.

Though the MT floor is, on average, more than 800 meters below the global mean for oceanic crust of similar age (Park et al., 1990), the seismic refraction study of Bibee et al. (1980) indicates a crustal thickness of 6–7 km, typical of normal oceanic crust. The range of spreading rates at 18°N (half-rates = 15–22 mm/a; Bibee et al., 1980; Hussong and Uyeda, 1981) is appropriate for slowly spreading mid-ocean ridges (Malinverno, 1993). Correspondingly, the axial morphology is characteristic of slow spreading ridges (Solomon and Toomey, 1992). An axial graben (12 to >20 km wide in the SMT and 10–15 km wide at 18°N) generally defines the spreading axis, within which an axial ridge ascends 200–700 meters above the valley floor (Barone et al., 1990). The axial ridge depth averages 3700 meters between 17°N and 16°N, deepening southward to 4500 meters near the southernmost sample locality at 15°N (Fig. 2). This change in bathymetric expression of the ridge correlates strongly with changes in basalt composition and we interpret this to reflect fundamental differences in magma generation along the ridge. The shallower ridge segment between 16° and 17°N and the deeper ridge segment between 16° and 15°N will be referred to as the N-SMT and S-SMT, respectively.

Early studies (Hart et al., 1972) showed the central portion of the MT to be underlain by young basaltic crust, corroborating the Karig (1971) proposal of formation by seafloor spreading. Trace element variations, REE patterns, and strontium isotopic compositions indicate affinities with MORB, rather than arc tholeiites (Hart et al., 1972). Lead isotopic studies also indicate a mantle source distinct from the source supplying Mariana arc lavas (Meijer, 1976). MT basalts are nevertheless distinguished from NMORB by high Al_2O_3/MgO, low FeO*/MgO (Fryer et al., 1981), and high H_2O (Garcia et al., 1979; Stolper and Newman, 1994). In addition, when normalized to HFSE abundances, LILE and LREE abundances for relatively primitive MT tholeiites are more than twice as high as NMORB (Fryer et al., 1981; Hawkins and Melchior, 1985). Based on the observation of similar basalts in other active back-arc basin settings, Fryer et al. (1981) proposed back-arc basin basalts (BABB) as a rock type distinct from MORB.

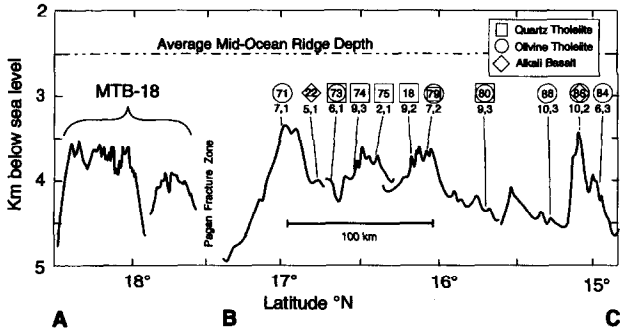

FIG. 2. Axial ridge depth of the SMT plus the intensely studied 18°N ridge sections. A, B, and C correspond to ridge segments located in Fig. 1. Dredge location markers are enclosed in symbols indicating major element normative compositions. Where two symbols are shown, the outer symbol indicates the dominant rock group. Numbers below dredge symbols correspond to # of glasses analyzed by electron microprobe, # of glasses analyzed for trace elements, and/or isotopes at UTD. Note that the ridge south of 16°N (S-SMT) is deeper by several hundred meters relative to the ridge segment to the north (N-SMT). The seamount sampled by D86 may be a slightly off-axis seamount.

More recent studies have extended the range of compositions sampled in the Mariana Trough. Basalt glasses very similar to arc tholeiites with respect to trace element and isotopic composition have been recovered at 18°N (MTB-18: Hawkins et al., 1990; Volpe et al., 1990). The MORB source at 18°N is isotopically like Indian Ocean mantle (Volpe et al., 1990 and Hickey-Vargas, 1991). Basalts collected at 22°N (MTB-22), where the Mariana Trough is narrow and thought to be young (Martinez et al., 1995), show a strong similarity to arc basalts (Stern et al., 1990).

3. SAMPLE LOCATIONS AND PETROGRAPHY

Eleven dredges recovered by the R/V Sonne during the Sonne 69 cruise in 1989 contained samples with basaltic glass. Dredge locations, depth ranges, and salient petrographic features are listed in Table 1. Dredge collections were classified onboard according to distinctive petrographic features visible in hand specimens, typically the type and amount of phenocrysts. The first number after the dredge number refers to the onboard suite designation and is followed by the within-suite sample number. The two dredges containing alkali basalts (D22 and D86) are located between (offset) ridge segment tips. All but one of the samples selected for trace element and isotopic analysis from the eleven dredges are pillow rind fragments; D71:1-7 is from a sheet flow. The samples typically contain less than 10 vol% vesicles. D74:2-3 and D75:1-1 contain greater than 15% vesicles. Olivine and plagioclase phenocrysts are typically present and make up less than 10% of the rock. In the S-SMT plagioclase is more abundant than olivine. The reverse is generally true for the N-SMT. Clinopyroxene is rare and commonly xenocrystic (i.e., resorbed or in a reaction relationship with the host). Clinopyroxene was not observed in any glassy pillow rind (vitrophyre).

4. SAMPLE PREPARATION AND ANALYSIS

Eighty glasses were analyzed for major elements at the Smithsonian Institution using an electron microprobe; analytical procedures are described in Melson et al. (1976). Mg# is calculated as 100(Mg/Mg+ Fe^{2+}), with Fe^{3+}/Fe^{2+} calculated by the algorithm of Kress and Carmichael (1988). The complete dataset is available from T. O'Hearn by email (MNHMS002@SIVM.SI.EDU) or on disk as an ASCII file or in Microsoft Excel format. From these samples, twenty-two glass samples were selected for trace element and isotopic analysis. These were processed first by picking +20 mesh chips with minimal surface alteration. The chips were then crushed and ultrasonicated in ethanol and examined under a microscope. Chips with weathered surfaces, devitrification spots, or phenocrysts were removed. Crushing, cleaning, and picking was continued at +40, +60, +100, and +120 mesh until the chips were sufficiently transparent to confirm that they were free of phenocrysts and devitrification spots. Prior to dissolution the glass samples were washed for two minutes in 2.5N HCl.

Approximately 100 mg and 70–100 mg of glass were dissolved for neodymium and strontium isotopic and trace element concentration analyses, respectively. Standard isotope dilution and cation exchange techniques were used to separate LILE (K, Rb, Sr, and Ba) and REE (La, Ce, Nd, Sm, Eu, Gd, Dy, Er, and Yb). A procedure modified after Richard et al. (1976) was used to further isolate Ba, La, and Ce for isotope dilution analysis and separate Nd from Sm for isotope composition runs. Lead analyses required 15–30 mg of glass for determination of concentration by isotope dilution and sufficient glass (70–270 mg) for a 90–100 ng processing load for isotope composition runs. The Pb separation procedure is reported in Manton (1988), with an initial anionic column separation. Total processing blanks were: Pb, less than 140 pg; Nd, less than 700 pg; and Sr, less than 2 ng. Blanks are less than 0.5 relative % for samples with the lowest concentrations of the elements analyzed (in all cases D84) except Rb (~2%). Strontium and neodymium isotopic compositions were determined with a Finnigan MAT 261 multi-collector thermal ionization mass spectrometer in dynamic mode. Strontium isotopic compositions were fractionation-corrected to $^{86}Sr/^{88}Sr = 0.1194$ and adjusted relative to E&A $SrCO_3$ $^{87}Sr/^{86}Sr = 0.70800$. Neodymium isotopic compositions were fractionation-corrected to $^{146}Nd/^{144}Nd = 0.7219$ and ϵ_{Nd} was calculated using the ϵ_{Nd} values of Pier et al. (1989) for BCR-1 and UCSD standards. The standard values with reproducibility during 18 months during which strontium and neodymium isotopic analyses were carried out (±2 s.d., with digits corresponding to the last decimel places reported) were: E&A $SrCO_3$ $^{87}Sr/^{86}Sr = 0.708027$ (39; $n = 38$), UCSD $^{143}Nd/^{144}Nd = 0.511826$ (25; $n = 36$), and BCR-1 $^{143}Nd/^{144}Nd = 0.512618$ (±19; $n = 9$). Lead was analyzed over a one week period, and after 0.15% per amu Pb fractionation correction, the average value for thirteen analyses of NBS 981 (±2 s.d.) was: $^{206}Pb/^{204}Pb = 16.936(20)$, $^{207}Pb/^{204}Pb = 15.481(19)$, $^{208}Pb/^{204}Pb = 36.692(52)$. For a subset of seventeen samples, H_2O and CO_2 were determined by Fourier transform infrared spectroscopic analysis of glass, following the general methods of Dixon et al. (1991) and modified by the use of a NicPlan microscope. Each sample was analyzed four times, using apertures ranging from 40 to 200 5m across and 1024–2048 scans. Thicknesses ranged from 54 to 319 5m. Uncertainties for water analyses (1 standard deviation of duplicate analyses) are less than ±0.16 wt%, generally less than ±0.10 wt%.

5. RESULTS

The eighty analyzed SMT glasses are basaltic. Except for dredge 80, which contains some samples with 53–55% SiO_2, all samples have ≤52.5% SiO_2 (normalized to 100% anhydrous). MgO, FeO*, and Al_2O_3 have similar ranges to MTB-18 glasses and Na_2O and TiO_2 abundances span the range defined by MTB-22 and MTB-18 (Fig. 3a,b). K_2O abundances are also similar to MTB-18 glasses except for D84 samples which have abundances typical of NMORB.

Based on normative compositions, the SMT basalt glasses can be divided into quartz and olivine tholeiites and subordinate alkali basalts. Olivine tholeiites display a greater range and greater average abundance of FeO*, Na_2O, and TiO_2 than quartz tholeiites and have from 1–12% normative olivine. The compositional range of the olivine tholeiites is similar to the most common basalt-type reported from 18°N (Hawkins et al., 1990). Quartz tholeiites are present only in the N-SMT and contain up to 3% normative quartz. A dominant subset of the quartz tholeiites resemble MTB-22 glasses in major, minor, and trace element composition (Stern et al.,

Table 1. Dredge samples, locations, and brief bathymetric and petrographic descriptions.

Dredge	Lat(°N)	Long(°E)	depth (meters)	Description	samp	% vesicles	% oliv	% plag
GTVA 71	16°59.11'	144°50.05'	3400	sheet flow; shoalest part of axial ridge segment	1-7	10	0.2	0.4
DS 22	16°57.38'	144°46.98'	3055	peak on structural high W.(?)	2-2	1	3	1
	16°57.93'	144°47.21'	3287	of active rift; fresh pillows				
GTVA 73	16°41.31'	144°48.46'	4236	small high between two deeps	2-2	4	7	1
	16°41.40'	144°50.13'	4125	in rift valley; sedimented				
DS 74	16°32.43'	144°51.02'	3600	small high in central rift;	2-1	16	5.2	2
	16°31.71'	144°50.98'	3709	fresh pillow fragments	2-3	25	10	5
					3-1	0.6	3	0.2
GTVA 75	16°24.29'	144°50.97'	3955	W. rift valley near tip of	1-1	16	7	<0.1
	16°24.51'	144°51.42'	3670	small OSC(?); minor Mn-stain				
DS 18	16°10.33'	144°47.14'	4052	small seamount, W. cent. rift	1-6	10	6	9
	16°10.91'	144°47.59'	3838	valley; glassy pillow fragments				
DS 79	16°04.77'	144°47.03'	3747	small seamount E. of rift	1-1	12	2	0.2
	16°04.81'	144°47.98'	3625	axis; glassy pillow fragments	2-2	10	0	0.4
DS 80	15°44.40'	144°45'	3730	corner high, W. side rift, N.	21-2	10	3	7
	15°45.79'	144°45'	3923	side transform; thin Mn-stain	23-2	10	7	8.4
					25-3	8	0	5
DS 89	15°23.65'	144°29.10'	4035	W. wall, rift valley; glass				
	15°23.70'	144°29.41	3100	fragments embedded in sandstone				
DS 88	15°17.80'	144°31.58	4671	large cone in rift valley;	1-2	2	1	2
	15°17.76'	144°30.56	4279	fresh pillows, minor sediment	2-1	10	2	4
					3-1	8	1	6
DS 86	15°05.30'	144°29.69'	3386	small high, short ridge segment	4-1	8	0	1.8
	15°05.10'	144°30'	3517	or rift terminus; pillows + sed.	6-1	2	tr	tr
DS 84	14°59.87'	144°29.56'	4272	axial high; glassy pillows,	1-1	4	3	15
	15°00.08'	144°25.69'	4046	minor sediment	2-1	4	3	15
					3-1	2	0	4.8

samp= samples analyzed for trace elements and isotopic compositions; OSC= overlapping spreading centers; tr= trace

1990) with distinctly lower TiO_2 and Na_2O at a given MgO (Fig. 3). The normative distinction of olivine from quartz tholeiite sometimes obscures the similarity of glasses in dredges containing both olivine and quartz normative tholeiites; that is, olivine and quartz tholeiites within a dredge suite may be related by fractionation. However, two fractionation trends can be identified when normative composition is plotted against Mg#: a high-Q trend defined by N-SMT samples and a low-Q trend defined by S-SMT samples (Fig. 4a). Other compositional features confirm that there is little compositional overlap among N-SMT and S-SMT olivine tholeiites. Olivine tholeiites from the N-SMT have lower TiO_2, Na_2O, (Fig. 3), and FeO* and higher Mg# (Fig. 4b,c) and higher K_2O at a given Mg# relative to S-SMT olivine tholeiites. D80 is especially interesting because it contains quartz tholeiites but is compositionally intermediate between samples from ridge segments north and south of it. Arc-like compositions similar to those recovered near 18°N (ALVIN Dive 1846; Hawkins et al., 1990) are not represented in the SMT sample set.

Recast into mineral compositions and projected into pseudo-ternary diagrams (Fig. 5), SMT glass trends parallel the 1 atm olivine-plagioclase-pyroxene cotectic of Tormey et al. (1987) but is displaced toward the 1 kb, water-saturated cotectic of Sisson and Grove (1993). Note that with the exception of D71 at the northern end of the N-SMT, there is a complete separation of N-SMT and S-SMT suites.

Twenty-two glass compositions selected for trace element and isotopic analysis include all dredges that contained glass while covering the compositional range observed in the major element dataset. Concentrations of trace elements are listed in Table 2 and shown in Fig. 6 normalized relative to average NMORB abundances (Hofmann, 1988). Except for D84 samples, all SMT samples are enriched in K, Rb, and Ba and Sr relative to NMORB. D84 samples are distinct from other Mariana Trough basalts and show smooth, NMORB-normalized element patterns that are depleted relative to NMORB. Excepting D84 and the alkali basalts, SMT samples also show positive anomalies in Pb. S-SMT tholeiites have higher concentrations of the heavy REE, and generally lower concentrations of Rb and Ba than N-SMT tholeiites (Fig. 6a). Normalized element patterns are similar for N-SMT olivine and quartz tholeiites except that olivine tholeiites have slightly lower abundances of LREE and LILE,

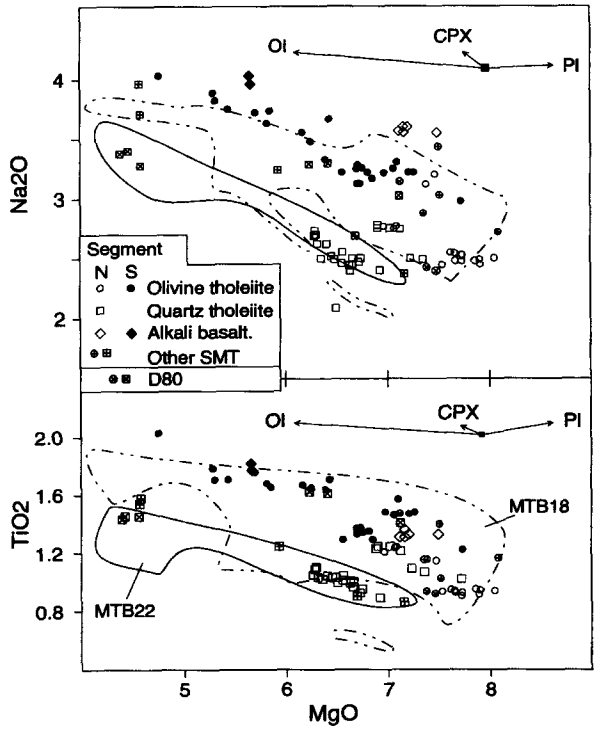

FIG. 3. The moderately incompatible elements Na_2O (a) and TiO_2 (b) vs. MgO for Mariana Trough glass data only. SMT glass data are divided into northern (N-SMT) and southern (S-SMT) segments and include all data collected by microprobe. The mineral fractionation arrows represent 5% fractionation of phenocryst core compositions from relatively primitive glasses analyzed by Hawkins and Melchior (1985). MTB18 data (that also include samples collected from the SMT and indicated as Other) are from Fryer et al. (1981), Hawkins and Melchior (1985), Volpe et al. (1987), and Hawkins et al. (1990). MTB22 data are from Stern et al., (1990). The small MTB-18 dashed field at very low Na and Ti enclose the unusual 'arc'-like samples of ALVIN 1846 (Hawkins et al., 1990). The symbols are the same as in Fig. 2 except solid circles for olivine tholeiites south of D80.

consistent with a fractionation relationship. D80:23-2 is distinctive in being the S-SMT tholeiite that has strong trace element and isotopic similarities with N-SMT tholeiites, including trace element abundance patterns (Fig. 6a). K/Rb is distinctly higher in S-SMT tholeiites (800–1100) relative to N-SMT tholeiites (400–740); D80:23-2 has a K/Rb of 560, like that of N-SMT tholeiites. Again with the exception of D80, K/Ba is lower in the N-SMT (35–53) relative to the S-SMT (61–88). Mean K/Rb and K/Ba for N-SMT tholeiites (549 and 44) approaches that for subaerial Mariana arc volcanoes (mean K/Rb = 500; K/Ba = 31; Chow et al., 1980), whereas (excepting D80) that for S-SMT tholeiites (mean K/Rb = 903; mean K/Ba = 77) is more similar to that of NMORB (K/Rb = 1070, K/Ba = 95; Sun and McDonough, 1989). Similarly, Sr/Nd in N-SMT tholeiites is higher (19–32) than S-SMT tholeiites (11–20, except for D80 with Sr/Nd = 25), and is another indication that N-SMT tholeiites contain a significant subduction component. Ce/Pb is slightly higher in S-SMT tholeiites (17–22, without D-80) than in N-SMT tholeiites (11–19), with the alkali basalt samples having the highest Ce/Pb (24–27).

All S-SMT and most N-SMT olivine tholeiites have concave-down REE patterns whereas quartz tholeiites commonly are enriched in the light REE (Fig. 7). REE abundances are generally higher for S-SMT relative to N-SMT basalts. The relative enrichment of heavy REE in S-SMT basalts is especially striking. N-SMT tholeiites commonly have negative Ce anomalies, a feature that is consistent with the participation of a subduction component (Hole et al., 1984); positive Eu anomalies may also reflect such effects. Such anomalies are not characteristic of S-SMT lavas.

Analyzed SMT glasses contain between 0.20 and 2.78 wt% H_2O and less than 228 ppm CO_2. This range is similar to but larger than that found for 11 MTB-18 glasses (0.49–2.14% H_2O, <175 ppm CO_2; Stolper and Newman, 1994). SMT and MTB-18 tholeiites plot in the H_2O-K_2O field defined for back-arc basin basalts by Muenow et al. (1990), very close to a line of K_2O/H_2O = 0.25. The glasses are approximately saturated in these volatiles but must have lost considerable amounts of CO_2 as CO_2 is quantitatively lost before water is affected (Delaney et al., 1978). For this reason the CO_2 data is not included in the following discussion, although the water contents are probably good approximations of the magmatic concentrations. The wide range of water contents correlates with normative composition (quartz tholeiite contain 1.2–2.8% H_2O; olivine tholeiite

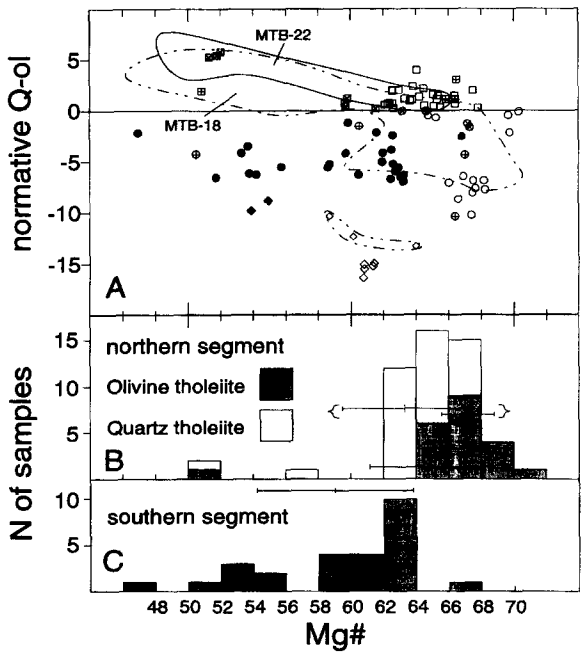

FIG. 4. (a) Plot of Mg# vs. (normative Quartz-normative Olivine). Mg# is calculated after Kress and Carmichael (1988) with T(°C) = 1200 and $f(O_2)$ = Ni/NiO − 0.6 log units. As in Fig. 3, dashed and solid fields are for MTB18 and MTB22, respectively. The small dash-enclosed field is for alkali basalts recovered near 18°N, not the 'Arc'-like samples, as in Fig. 3. (b) and (c) are Mg# histograms of the northern and southern SMT segment basalts, respectively. Note the tighter clustering and higher Mg# of the northern section, including the quartz tholeiites. The mean ± 1 s.d. are shown for the northern and southern sections and bracketed for quartz and olivine tholeiite in the northern section.

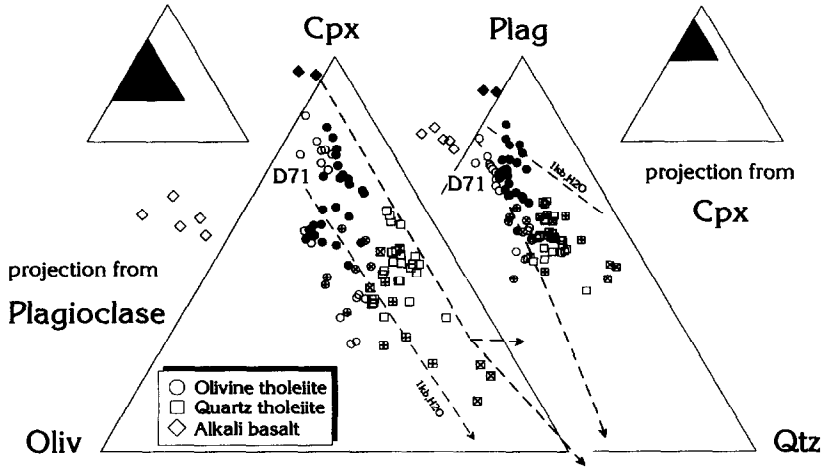

FIG. 5. Plagioclase and cpx projections. The thick dashed line is the 1 atm, 3 phase cotectic determined by Tormey et al. (1987). The thin dashed line labeled "1kb,H2O" is a line through 3 phase plus glass assemblages at 1 kb P_{H_2O} from Sisson and Grove (1993). Symbols are as in Fig. 3.

contain 0.2–1.5% H_2O) and incompatible element concentrations but inversely correlate with ridge depth (deeper ridge segments are drier). Water covaries strongly with other indications of the subduction component, for example K/Rb (Fig. 8).

The range of isotopic compositions for SMT samples is

Table 2. Glasses with trace element and/or isotopic analyses.

	Northern SMT													
Sample	71:1-7	22:2-2	73:2-2	74:2-1	74:2-3	74:3-1	75:1-1	18:1-6	18:3-2	79:1-1	79:2-2	80:21-2	80:23-2	80:25-3
Lat(°N)	16.99	16.96	16.69	16.53	16.53	16.53	16.41	16.18	16.18	16.08	16.08	15.76	15.76	15.76
SiO_2	49.36	49.30	51.18	51.37	50.78	51.64	51.22	50.92	51.3	51.08	50.43	52.19	50.59	53.84
TiO_2	0.90	1.36	1.25	0.89	1.05	1.22	1.07	0.97	0.99	0.91	1.16	1.62	0.94	1.46
Al_2O_3	16.79	17.40	16.89	17.24	16.72	16.70	17.06	16.77	16.56	17.75	16.87	15.88	17.13	16.16
FeO*	7.64	9.54	8.16	7.01	7.96	7.96	8.04	8.02	7.68	6.98	8.05	9.20	7.62	8.96
MgO	7.74	7.17	7.09	6.93	6.29	7.13	6.30	6.66	6.51	7.91	7.39	6.42	7.40	4.58
CaO	13.17	10.74	11.22	11.82	12.00	11.06	11.33	12.09	11.78	11.54	11.30	10.73	12.48	8.96
Na_2O	2.48	3.60	2.77	2.40	2.69	2.74	2.73	2.44	2.09	2.49	3.12	3.30	2.43	3.28
K_2O	0.26	0.22	0.32	0.28	0.32	0.30	0.51	0.32	0.31	0.23	0.27	0.28	0.24	0.63
P_2O_5	0.14	0.14	0.18	0.13	0.18	0.17	0.17	0.12	0.13	0.14	0.11	0.16	0.11	0.21
H_2O	1.34	0.48	1.46	2.08	2.16	1.18	2.21	2.03			0.97		1.52	2.78
Sum	99.82	99.95	100.52	100.15	100.15	100.10	100.64	100.34	97.35	99.03	99.67	99.78	100.46	100.86
Mg#	68	61	65	68	63	65	62	64	64	70	66	60	67	52
Type	OT	AB	OT	QT	QT	QT	QT	QT	QT	OT	OT	QT	OT	QT
K	2030	1870	2520	2470	2720	2660	4190	2330		2000	2100		1800	
Rb	2.75	1.41	4.25	5.11	6.34	4.02	10.4	4.95		4.41	3.41		3.19	
Sr	232	269	188	203	306	185	284	210		160	202		165	
Ba	43.5	17.0	61.7	71.2	50.9	56.1	103	66.1		49.9	39.3		41.1	
La	3.70	4.49	4.57	4.57	4.92	4.77	6.53	4.00		3.33	4.15		3.26	
Ce	9.38	11.8	12.1	9.36	12.9	12.5	14.8	9.74		8.65	11.6		7.85	
Nd	7.40	8.19	9.63	7.07	10.0	9.55	10.6	7.65		7.52	9.22		6.52	
Sm	2.27	2.50	2.87	2.23	2.91	3.01	3.05	2.46		2.58	2.88		2.10	
Eu	0.909	1.06	1.15	0.855	1.12	1.12	1.1	0.961		0.997	1.12		0.841	
Gd	2.91	3.39	4.10	3.02	3.57	3.97	3.66	3.45		3.53	4.12		3.01	
Dy	3.22	3.92	4.47	3.43	3.91	4.45	4.01	3.82		4.22	4.37		3.50	
Er	1.92	2.41	2.88	2.18	2.35	2.78	2.42	2.45		2.64	2.64		2.18	
Yb	1.89	2.34	2.80	2.07	2.27	2.63	2.4	2.37		2.63	2.54		2.12	
Pb	0.63	0.50	0.75	0.89	0.65	0.83	1.38	0.74		0.69	0.63		0.67	1.46
$^{206}Pb/^{204}Pb$	18.220	17.831	18.404	18.543	18.459	18.349	18.598	18.509	18.662	18.325	18.240		18.366	
$^{207}Pb/^{204}Pb$	15.448	15.441	15.519	15.498	15.500	15.550	15.512	15.509	15.54	15.471	15.487		15.517	
$^{208}Pb/^{204}Pb$	37.859	37.685	38.087	38.129	38.080	38.094	38.200	38.153	38.244	38.006	37.899		38.077	
$^{87}Sr/^{86}Sr$	0.70280	0.70287	0.70289	0.70298	0.70273	0.70284	0.70307	0.70304	0.70300	0.70292	0.70274	0.70289	0.70292	0.70306
$^{43}Nd/^{144}Nd$	0.513025	0.513005	0.513073	0.513049	0.513055	0.513088	0.512980	0.513040	0.513066	0.513087	0.513136	0.513156	0.513090	0.513029
εNd	8.1	7.7	9	8.5	8.7	9.3	7.2	8.4	8.6	9.3	10	10.6	9.4	8.2

OT= olivine tholeiite; QT= quartz tholeiite; AB= alkali basalt

Table 2. Continued.

	Southern SMT							
Sample	88;1-2	88;2-1	88;3-1	86;4-1	86;6-1	84;1-1	84;2-1	84;3-1
Lat(°N)	15.30	15.30	15.30	15.08	15.08	15.01	15.01	15.01
SiO_2	50.77	50.71	49.96	51.05	51.57	51.04	51.29	51.32
TiO_2	1.68	1.35	1.30	1.83	1.72	1.58	1.48	1.23
Al_2O_3	16.12	16.83	17.02	15.03	15.42	15.34	15.40	16.38
FeO*	8.86	8.51	8.41	10.01	9.67	9.89	9.43	8.08
MgO	6.18	6.72	6.86	5.66	6.44	7.11	7.22	7.74
CaO	10.55	11.12	11.08	10.68	10.90	11.81	11.69	11.36
Na_2O	3.56	3.13	3.17	4.03	3.67	3.31	3.22	2.98
K_2O	0.31	0.28	0.28	0.45	0.26	0.06	0.07	0.12
P_2O_5	0.20	0.15	0.16	0.19	0.18	0.13	0.15	0.14
H_2O	1.3	1.04	1.23	0.58		0.2	0.21	
Sum	99.53	99.84	99.47	99.51	99.83	100.47	100.16	99.35
Mg#	60	63	63	55	59	61	62	67
Type	OT	OT	OT	AB	OT	OT	OT	OT
K	3120	2790	2640	3370	2540	480	460	
Rb	3.54	3.35	3.25	2.88	2.31	0.54	0.51	
Sr	197	202	205	217	197	99.8	97.1	
Ba	41.4	43.9	43.3	35.4	28.8	5.45	5.47	
La	6.34	5.4	5.16	6.68	5.85	2.00	2.07	
Ce	17.0	14.4	13.9	17.5	16.9	7.82	7.84	
Nd	12.9	10.9	10.5	13.4	13.4	8.91	9.00	
Sm	3.98	3.32	3.29	3.93	4.24	3.27	3.26	
Eu	1.43	1.29	1.25	1.56	1.59	1.23	1.25	
Gd	5.08	4.43	4.15	4.96	5.75	4.39	4.55	
Dy	5.87	4.96	4.78	5.59	6.14	5.38	5.37	
Er	3.63	3.06	3.00	3.40	3.83	3.31	3.40	
Yb	3.54	2.94	2.91	3.21	3.62	3.20	3.16	
Pb	0.89	0.70	0.83	0.66	0.78	0.38	0.38	0.32
$^{205}Pb/^{204}Pb$	18.072			17.831	17.807	17.723	17.719	
$^{207}Pb/^{204}Pb$	15.504			15.426	15.402	15.414	15.422	
$^{208}Pb/^{204}Pb$	37.881			37.556	37.488	37.398	37.402	
$^{87}Sr/^{86}Sr$	0.70286	0.70289	0.70290	0.70279	0.70283	0.70248	0.70253	0.70268
$^{143}Nd/^{144}Nd$	0.513083	0.513082	0.513080	0.513072	0.513106	0.513184	0.513201	0.513146
εNd	9.2	9.2	9.2	9	9.7	11.2	11.5	10.4

similar to that at 18°N but extended by D84 samples to lower $^{87}Sr/^{86}Sr$ and higher ϵ_{Nd} (Fig. 9). No SMT samples have as 'arc'-like an isotopic signature as that reported for the 'arc'-like suite (A 1846) at 18°N (Volpe et al., 1990). SMT samples bracket 18°N samples and extend the known range of Mariana Trough basalts. These new data for N-SMT glasses also broadens the Mariana Trough field perpendicular to the mantle array. If the 'arc'-like sample from 18°N is excluded, the SMT and MTB-18 span a similar range in $^{206}Pb/^{204}Pb$, from about 17.72–18.6 (Fig. 10). The very large variation in $^{206}Pb/^{204}Pb$ for the MTB contrasts sharply with the much more homogeneous $^{206}Pb/^{204}Pb$ found for Mariana arc lavas. An unexpected result is the separation (excepting D80) of N- from S-SMT tholeiites in $^{206}Pb/^{204}Pb$ space, with S-SMT tholeiites having $^{206}Pb/^{204}Pb < 18.1$ and N-SMT tholeiites having $^{206}Pb/^{204}Pb > 18.2$. D80 is again distinctive in being the S-SMT tholeiite that is very similar to N-SMT tholeiites. The two alkali basalt samples are isotopically similar in having the low $^{206}Pb/^{204}Pb$ (17.8) characteristic of S-SMT basalts. In lead-lead (Fig. 10b,c) and $^{87}Sr/^{86}Sr$-$^{206}Pb/^{204}Pb$ (Fig. 10a) diagrams, alkali basalts, and S-SMT tholeiites have the relatively high $^{208}Pb/^{204}Pb$ typical of Indian Ocean MORB and generally lie outside the field for Pacific MORB. The N-SMT suite extend into the least radiogenic part of the MTB-22 and Mariana arc CIP field, but again are not as 'arc'-like as the unusual sample from 18°N (Volpe et al., 1990).

6. DISCUSSION

MT basalts completely span the compositional and isotopic space between MORB and Mariana arc basalts. It is important to understand what controls these variations, because MTB is clearly a hybrid, and like all hybrids, offers insights into both of its parents. In this case, the role of the parent is played by MORB and arc sources and processes of melt generation.

The approach we adopt here is to focus on an intermediate length scale appropriate for understanding SMT heterogeneities. First-order bathymetric and geochemical variations observed for SMT basalts indicate that this heterogeneity has a wavelength on the order of 100 km. This is intermediate between the within-segment scale (1–10 km wavelength) previously defined at 18°N (Volpe et al., 1990) and the basinwide scale observed for basalts erupted along the length of the MT (ca. 1000 km wavelength; Stern et al., 1990). The SMT dataset provides an especially useful perspective because, as we show below, the heterogeneity correlates simply with variations in the degree of melting.

In this discussion we concentrate on understanding the origin of SMT heterogeneity. This is done first by examining the nature of the unmodified mantle component. We then demonstrate that some of the geochemical variation is due to the degree of melting but that most of the variability requires modification of asthenospheric MORB-like mantle by a hydrous fluxing agent.

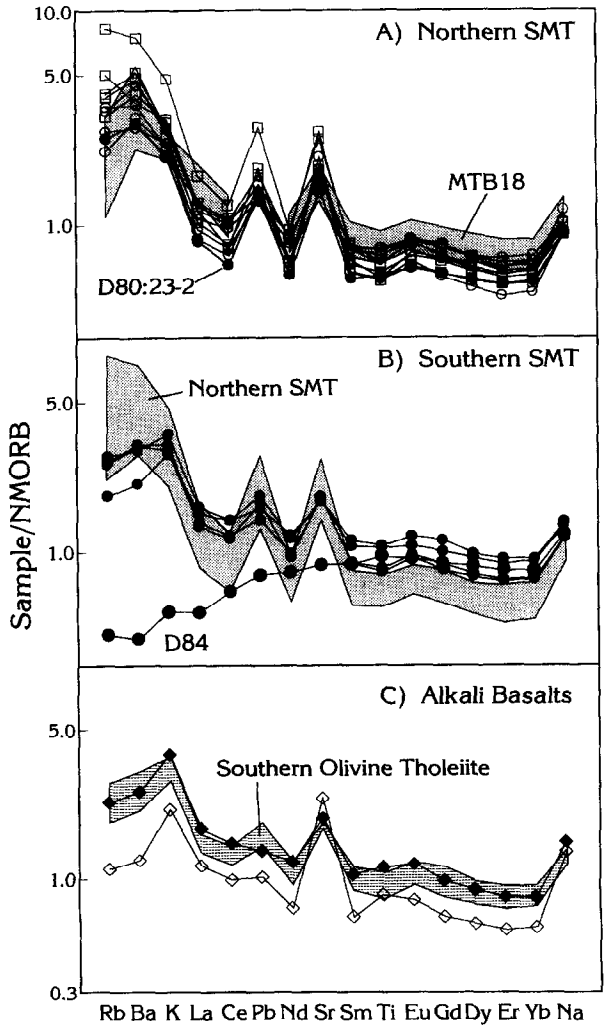

FIG. 6. NMORB-normalized compatibility diagram after Hofmann (1988) showing: (a) olivine and quartz tholeiites from the northern SMT section compared with a partial field (no Pb) for MTB18; (b) S-SMT olivine tholeiites compared with the field for N-SMT basalts; (c) alkali basalts compared with the field for S-SMT basalts (no D84). Symbols are simplified from those in Fig. 3: open symbols = N-SMT, filled = S-SMT. Circle = olivine tholeiite, square = quartz tholeiite, diamond = alkali basalt. Note that even though D80:23-2 is geographically part of the SMT, chemically it looks similar to the N-SMT suite. The curve labeled 'D84' is the average of two very similar samples, 84:1-1 and 84:2-1.

6.1. Nature of the Unmodified MTB Mantle

The SMT dredge suite includes the most MORB-like samples (D84) yet recovered from the Mariana Trough. These are more depleted in LIL and LRE elements than the typical N-MORB of Hofmann (1988) and are similar to the N-MORB of Sun and McDonough (1989). This suite also contains by far the lowest H_2O for any MTB, with 0.2% water. This compares with 0.49% for the driest sample at 18°N (Stolper and Newman, 1994) and the next driest SMT tholeiite (D79: 0.97%). The water content in D84 basalts is similar to that of MORB (≤0.21%, Michael, 1988) and suggests the subduction component is negligible for these samples. This provides us with a valuable opportunity to characterize a piece of unmodified mantle beneath the Mariana Trough and examine the suggestion that the unmodified mantle source Mariana Trough basalt is similar to Indian Ocean-type asthenosphere (Volpe et al., 1990; Hickey-Vargas et al., 1995).

The isotopic characteristics of the D84 suite are consistent with derivation from a long-depleted source remarkably similar to the typical N-MORB source of Hart (1988), especially with respect to strontium and neodymium isotopic compositions. The suite contains Pb as unradiogenic as any MTB with $^{206}Pb/^{204}Pb$ lower than reported for Pacific MORB (Mahoney et al., 1994). $^{208}Pb/^{204}Pb$ is above the Northern Hemisphere Reference Line (Hart, 1984), approaching the fields of proximal Indian Ocean MORB (Fig. 10). D84 and other SMT data do not clearly lie within the field of Indian Ocean MORB but often are intermediate between the fields of Pacific and Indian Ocean MORB (Fig. 9). The strontium and neodymium isotopic composition of the D84 is in the range reported for Pacific rather than proximal Indian Ocean MORB. This is also true for the N-MORB suite of Volpe et al. (1990). We conclude that the unmodified mantle source sampled by the D84 suite is unequivocally MORB-like, and that this mantle source is isotopically similar to, but not indistinguishable from, the Indian Ocean MORB source. We are intrigued by the fact that

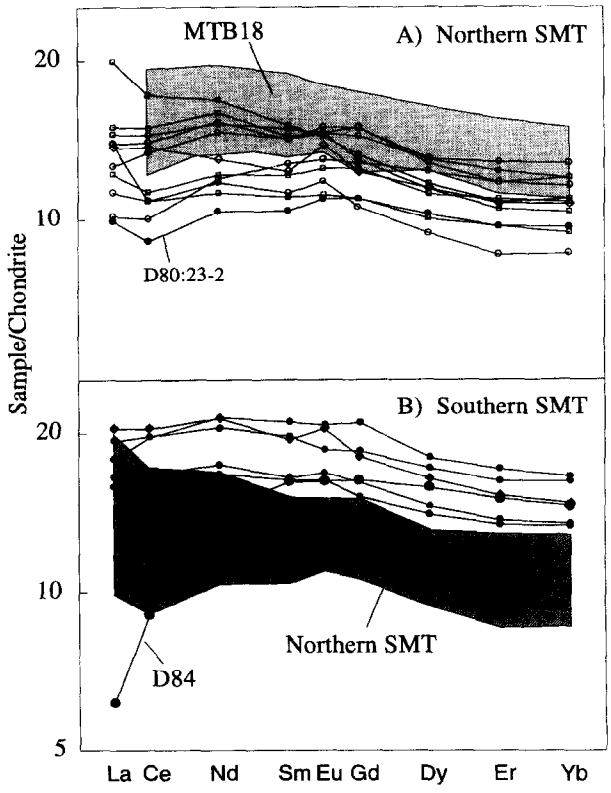

FIG. 7. REE patterns for basalts from (a) the northern SMT and D80:23-2, and (b) the southern SMT. The field shown for MTB-18 in (a) is from various literature sources. The field for northern SMT is shown for the sake of comparison in (b). Note that S-SMT basalts have much higher concentrations of HREE relative to N-SMT. Symbols as in Fig. 6.

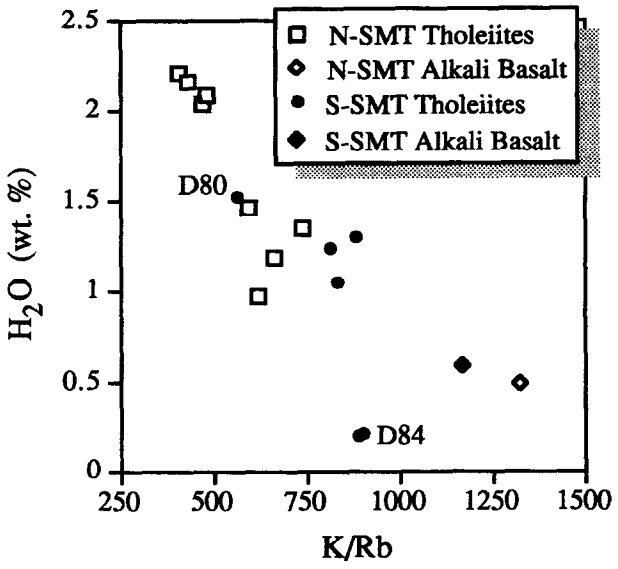

FIG. 8. Plot of water vs. K/Rb for SMT basalts. Note the strong anti-variation of K/Rb and water contents.

the most MORB-like sample ever recovered from the Mariana Trough is found at the southern extreme of our samplings, and we wonder if similar MORB-like basalts are erupted along the unsampled part of the extension axis farther south.

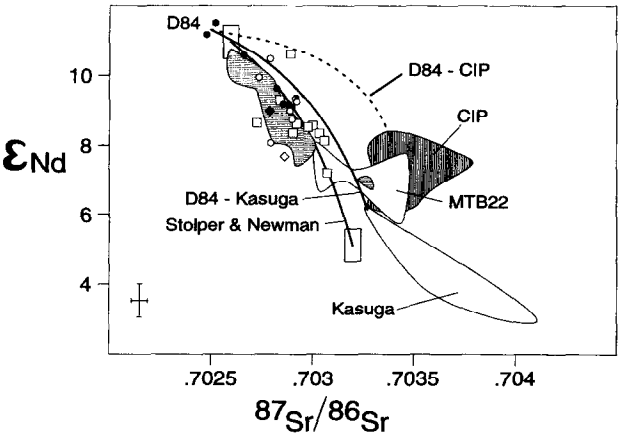

FIG. 9. ϵ_{Nd} vs. $^{87}Sr/^{86}Sr$. The horizontally-ruled field is defined by MTB-18 data (Volpe et al., 1990); note the position of very arc-like MTB-18 samples about $\epsilon_{Nd} = +7$ and $^{87}Sr/^{86}Sr = 0.7034$. MTB-22 data are from Stern et al. (1990). Data for the Mariana Arc Central Island Province (CIP) are from Lin et al. (1990) and sources listed therein. The Kasuga field is from Stern et al. (1993). Note that the two D84 samples have the highest ϵ_{Nd} and lowest $^{87}Sr/^{86}Sr$ reported for any Mariana Trough basalt. Also shown are three hypothetical mixing curves. The solid line labeled 'Stolper & Newman' refers to their fit to the MTB-18 data (Stolper and Newman, 1994, with boxes specified by their uncertainty). The solid line labeled 'D84-Kasuga' is a mixture of the average D84 basalt (Sr and Nd concentrations from Table 2) and Kasuga cross-chain sample K3:1885-4 (Stern et al., 1993). The dashed line labeled 'D84-CIP' is a mixture between D84 and an average of CIP compositions. Symbols as in Fig. 6. Typical analytical uncertainties are shown in the lower left.

6.2. Variations in the Extent of Partial Melting

The first-order variations in ridge axis depth along the SMT are most simply interpreted to result from different degrees of melting, as argued for mid-ocean spreading ridges (Klein and Langmuir, 1987). The S-SMT is 200 m to 800 m deeper than the N-SMT and this probably reflects significantly lower degrees of melting (fraction of melt extracted

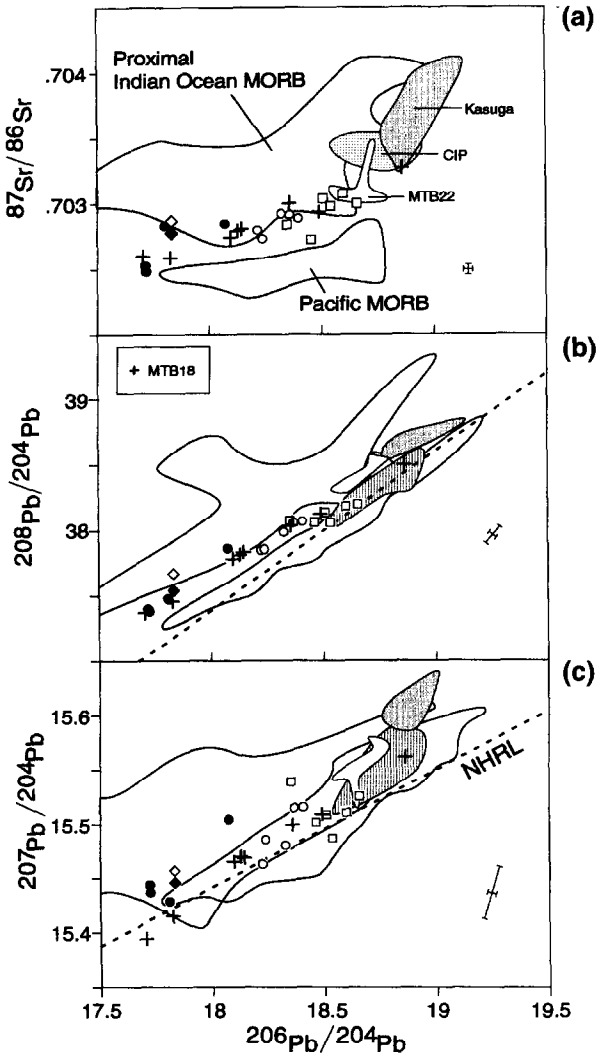

FIG. 10. Lead isotopes and $^{87}Sr/^{86}Sr$ vs. $^{206}Pb/^{204}Pb$ plots. The 'Northern Hemisphere Reference Line' of Hart (1984; NHRL) is indicated by a dashed line in the Pb-Pb plots. Crosses indicate MTB18 data (Volpe et al., 1990). The 'arc-like' sample (A-1846-9) has the highest $^{206}Pb/^{204}Pb$ of any MTB-18 sample and plots in the field for CIP lavas. Data for MTB-22 is from Stern et al. (1990). Data for the Kasugas is from Stern et al. (1993). Data for the Mariana CIP are from Meijer (1976) and Woodhead and Fraser (1985). Data for Pacific MORB are from the data and compilation of Mahoney et al. (1994). Data for the Indian Ocean includes the Southeast Indian Ridge, Central Indian Ridge, Ninetyeast Ridge, and Rodrigues Triple Junction. The Indian Ocean field does not include the SW Indian Ridge, which is geographically far removed from the Marianas and isotopically transitional to Atlantic MORB, and so is labeled Proximal IOMORB. References are in Mahoney et al. (1992). Symbols as in Fig. 6.

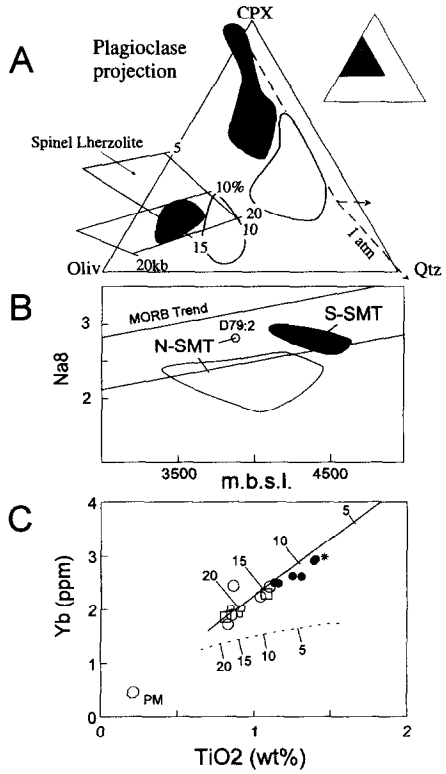

FIG. 11. (a) Plagioclase projection as in Fig. 5. Shaded and open regions bound the S- and N-SMT fields, respectively. Note that D86 samples are omitted, because these may sample an off-axis seamount. Isobaric, accumulated primary melts in the spinel lherzolite fields from Kinzler and Grove (1992) are gridded by pressure (Kbar) and percent melt. Primary melt compositions are calculated by olivine-only addition only for the relatively primitive SMT samples (Mg# > 65). The alkali basalts and S-SMT glasses extending along the 1 atm cotectic toward the plane of critical saturation have Mg#'s less than 65; (b) Na_2O abundances corrected for fractionation to 8% MgO (after Klein and Langmuir, 1987) are shown vs. estimated axial valley depth. The two lines bound the range for MORB reported in Klein and Langmuir (1987). N- and S-SMT samples are enclosed in distinct fields. Note that one suite of D79 from the N-SMT is geochemically similar to S-SMT basalts, (c) Degree of melting estimated from TiO_2 vs Yb variations. Symbols as in Fig. 6, with the following modifications: Large symbols correspond to samples with Mg# > 65, small symbols correspond to samples with Mg# = 60–65, and one sample marked with (*) has Mg# = 59. The compositions are corrected for olivine-only fractionation with $K_d(ol) = 0.015$, 0.03 for TiO_2 and Yb, respectively. Fractionation of CPX and PLAG are not corrected for and, if important, would lead to underestimation of F from this figure. The solid line is a spinel lherzolite non-modal melting curve labeled with degrees of F. Values of C_o = 0.217% TiO_2 and 0.493 ppm Yb (Sun and McDonough, 1989), D_o = 0.094 & 0.10 for a lherzolite (ol:opx:cpx of 60:30:10), and P = 0.275 & 0.31 for ol:opx:cpx melting proportions of 0:50:50. The dashed line is a garnet lherzolite melt curve with ol:opx:cpx:gar composition and melt proportion of 50:30:18:2 and 0:48:48:4, respectively. D_o and P for TiO_2 & Yb are 0.138 & 0.229 and 0.288 & 0.66, respectively.

per unit volume of mantle, or 'F') for the S-SMT relative to the N-SMT.

This inference is supported by estimates of F deduced from basalt chemistry. First, whereas normative compositions indicate that N-SMT basalts are down-temperature along the three phase cotectic relative to S-SMT glasses (Fig. 11a), the former have higher Mg#'s than the latter (Fig. 4). This suggests that contrasting major element compositions result from differences in melting conditions rather than fractionation. Because plagioclase joins olivine on the liquidus at about Mg# = 65 (Sinton and Fryer, 1987; note that different algorithims mean that the Mg# that we calculate is on average +3 relative to theirs), we have selected a subset of samples with Mg# > 65 to correct for olivine fractionation in a manner similar to that reported in Stolper and Newman (1994). Major element trends for this subset are indistinguishable from the MTB-18 suite studied by Stolper and Newman (1994). Quartz tholeiites and D71 olivine tholeiites from the N-SMT lie at the low TiO_2, high MgO end of the array interpreted to represent the high degree melting endpoint of the MTB-18 suite (Stolper and Newman, 1994).

Isobaric accumulated melt fractions after Kinzler and Grove (1992) are shown bounding a grid defined by pressure and %-melting of spinel lherzolite (Fig. 11a). The olivine-only fractionation corrections yield maximum estimates of 10–18% melting at ≥12 Kb for S-SMT samples and ≥15% melting at ≤15 Kb for N-SMT samples. The conclusion that S-SMT tholeiites reflect lower degrees of melting than do N-SMT tholeiites is complicated only by the D71 olivine tholeiites which project to the low pressure, low %-melting portion of the grid.

Sodium contents in MORB vary inversely with F (Klein and Langmuir, 1987). However, if metasomatism of the MTB mantle source by Na_2O-rich fluids has occurred (Stolper and Newman, 1994), the F-Na relationship would be altered such that only minimum estimates of degree of melting can be inferred from sodium contents. The S-SMT is characterized by higher (>2.5%) $Na_{8.0}$ (fractionation correction to MgO = 8.0 wt%, Klein and Langmuir, 1987) relative to the N-SMT (<2.5%) (Fig. 11b). The only exception to this rule is the D79:2 suite, recovered at the southern end of the N-SMT (Fig. 2), which has a higher $Na_{8.0}$ for its depth. Consideration of $Na_{8.0}$ values indicates that N-SMT basalts are most simply interpreted as higher degree melts than S-SMT basalts. It is noteworthy that S-SMT tholeiites plot in the MORB trend field of Klein and Langmuir (1987), defined on the basis of the global covariation of $Na_{8.0}$ and ridge depth, whereas N-SMT basalts often plot below the field. This may be due to the delayed appearance of plagioclase on the liquidus of water-rich BABB.

Similar variations in F are also inferred from trace element abundances. HREE concentrations are higher in S-SMT samples than in N-SMT (Fig. 7). Flat HREE patterns and pressure estimates from Fig. 11a indicate melting took place at depths shallower than the stability field of garnet lherzolite so that F should vary inversely with HREE concentrations. Titanium acts as an incompatible element under these conditions of mantle melting as well. We have used abundances of Yb and TiO_2 to quantify F for the SMT. These elements were chosen because source mixing may result in significant changes in source compositions for the minor and trace incompatible elements but should have little effect on HFSE such as Ti and Yb. Fractionation involving CPX will affect the abundances of Ti and Yb in the melt, but no indications

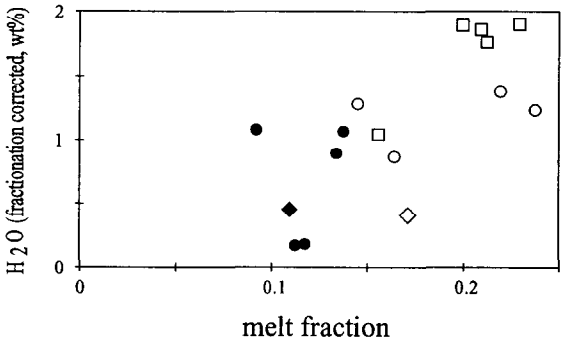

FIG. 12. Variation of water and degree of melting 'F.' Water contents have been corrected for olivine fractionation. Fractionation of CPX and PLAG are not corrected for and, if important, would lead to overestimation of water contents in the sample. Note the generally strong covariation of degree of melting with water contents. Uncertainties for water concentrations are less than ±0.16%. Symbols as in Fig. 6.

of CPX crystallization were noted petrographically. A simple forward model of non-modal batch melting of spinel lherzolite is shown as a trajectory superimposed on olivine-only fractionation-corrected samples (Fig. 11c). The calculated melt trajectory is consistent with the evolution of SMT tholeiites, although the alkali basalts (not shown) fall off this trajectory. This model yields estimates for F consistent with inferences from bathymetry and other geochemical considerations. Specifically, S-SMT tholeiites were derived by lower degrees (8–14%) of spinel lherzolite melting, whereas N-SMT basalts record higher degrees (14–23%) of melting.

6.3. Southern Mariana Trough Basalts and the BABB Paradox

A basic tenet of basalt petrogenesis is that, if the effects of fractionation and contamination can be neglected, incompatible element concentrations are functionally related to the degree of source melting. The simplest expression of this relationship is that concentrations of perfectly incompatible elements vary inversely with F; for closed-system melting of a homogeneous source, the greater the degree of melting, the lower the concentration of incompatible elements in the melt. The BABB paradox is that, for MTB and other BABB, the abundance of incompatible elements in these melts varies directly, rather than inversely, with F. This is a significant departure from the standard basalt petrogenetic model. Similar relationships observed for arc magmatism have been proposed to result from introduction of hydrous fluids beneath the arc that lower melting temperature while enriching the mantle in incompatible elements. Physical models for this fundamentally open-system process have been developed (Davies and Bickle, 1991; Davies and Stevenson, 1992). We call this process 'flux melting'. Flux melting contrasts with decompression melting, which approximates a closed-system process.

BABB are also paradoxical because they erupt at spreading ridges morphologically indistinguishable from those that erupt MORB, which form due to decompression melting. Despite this similarity, BABB show strong indications that incompatible and other elements have been introduced where melting occurs. We note that, although it is true that the cause of melting and metasomatism may be unrelated, or that the timing of these events may be significantly different, we find it simplest and, therefore, most attractive to think that the fluids carrying the LIL and other elements are introduced by the same hydrous melt or fluid that triggers melting. Support for this suggestion comes from the strong covariation of water content in the basaltic glass and independant estimates of the degree of melting (Fig. 12).

We use estimates of F derived in the previous section to examine the relationship between expected and observed incompatible element concentrations. Figure 13 shows this relationship, where the extent of melting (F) is plotted on the horizontal axis and the vertical axis values are ratios of the observed concentration of elements of interest divided by the concentration predicted from a closed-system, batch

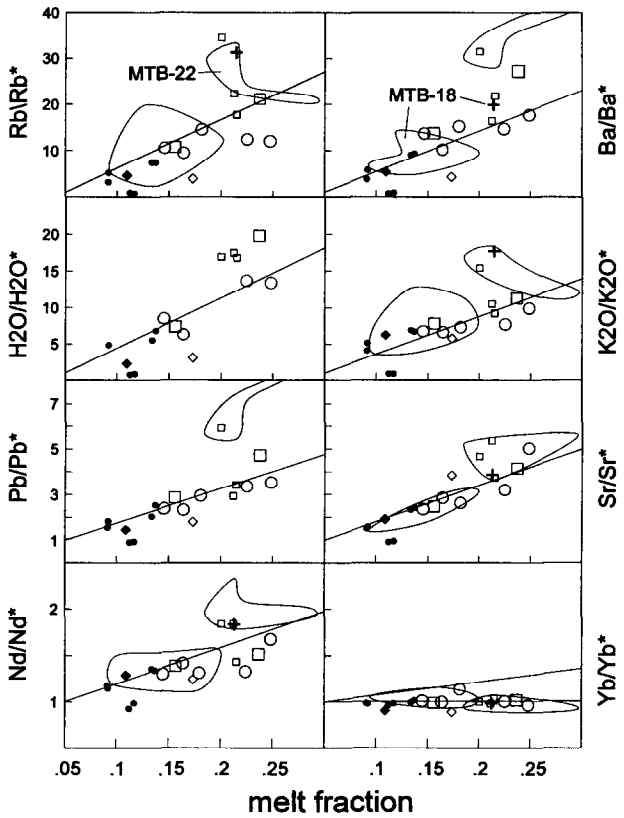

FIG. 13. Variations in the abundance of incompatible elements vs. F. Concentrations in samples are corrected for fractionation (numerator) and divided by the concentration expected from batch melting of a spinel lherzolite source appropriate for generation of D84 NMORB (asterisk-marked denominator). F for each sample is obtained from Fig. 10c. The observed/predicted ratio should equal one for any value of F in perfect, closed-system melting. The solid lines are the correlation of the amount of a H_2O-rich component with the degree of melting as calculated by Stolper and Newman (1994, Fig. 6). The line shown for Yb is an estimate based on the mixing endmembers for Y in Stolper and Newman (1994) and the expected correlation of Y and Yb. Symbols as in Fig. 6, except that large symbols correspond to Mg# > 65 and small symbols correspond to Mg# < 65.

melting model (e.g., Rb/Rb*). The LILE, Rb and Ba, are enriched up to about thirty-five times that expected for closed-system melting, whereas Yb shows no enrichment. Other elements show significant enrichments over that predicted (e.g., observed/expected ratios are $H_2O \leq 20$, $K \leq 15$, Pb & $Sr \leq 5$, and $Nd \leq 2$). The contrast in behavior between strong enrichments in LILE and no enrichment in moderately incompatible HFSE is consistent with introduction into the source of melting of hydrous fluids with high concentrations of water-soluble elements (e.g., the alkali metals) but low concentrations of water-insoluble elements such as the HFSE (e.g., Tatsumi et al., 1986).

The SMT data lead us to reject models whereby the subduction component is introduced by interaction of MORB-type magma with arc lithosphere. Our data confirm the importance of mixing in the generation of MTB (Volpe et al., 1987, 1990), but the conclusion that the arc component was old lithosphere trapped in the back-arc basin is unconvincing for the SMT, for tectonic and isotopic reasons. The tectonic argument concerns the ca. 100 km-long wavelength of the heterogeneity observed in the SMT. Trapped lithosphere could locally persist near the spreading axis but continued spreading must move material away from the spreading axis. We think that it is unlikely that suitably large lithospheric fragments (>100 km long) would persist at the widest, most mature part of the Mariana Trough. The isotopic argument is that arc lithosphere contains more radiogenic Sr than required by the subduction component of plausible models. Arc crust and lithosphere should be dominated by the trace element signature of the magmatic front. These lavas are characterized by relatively radiogenic Sr at a given neodymium or lead isotopic composition (Front Arc Trend of Stern et al., 1993). This inconsistency is shown on Figs. 4 and 5 of Volpe et al. (1987) and is reproduced in our isotopic mixing models (Fig. 9), where the Stolper and Newman (1994) model require that the isotopic composition of Sr in the enriched endmember lies below the mantle array. Mixing of MORB melts with arc lithosphere and crust, even if fresh, is thus inconsistent with the isotopic data. Alteration accompanying hydration is necessary for arc lithosphere to be the source of water for BABB. This alteration will result in more radiogenic Sr than fresh material, reinforcing the argument. The isotopic argument does not apply to arc magmas generated behind the magmatic front, such as the Kasuga cross-chain, which produce magmas with relatively nonradiogenic Sr (Rear-Arc Trend of Stern et al., 1993); we will return to this point shortly.

6.4. Further Constraints of the Nature of the Enriched Component

We conclude that melting is linked to a metasomatic event that both enhances melting and enriches the mantle source. For brevity, we refer this as the hydrous fluxing agent, or HFA. It is less apparent whether the HFA is a supercritical fluid (e.g., Saunders et al., 1991), or is water-rich melt. Either material could explain the chemical features described above. It may be misleading to represent the range of possible solutions by these endmembers; at the pressures and temperatures of interest there may be little difference between the properties of a silica-rich hydrous fluid and a hydrous magma, for example, water saturated melts at ≥ 2 GPa (corresponding to depths of about 65 km in the mantle) contain about 20 wt% H_2O (Thompson, 1992); Davies and Stevenson (1992) conclude that the distinction is irrelevant. In spite of this ambiguity, it is worthwhile to examine more carefully the constraints we have on the nature of the HFA responsible for generation of SMT basalts.

The combined mixing-melting calculation of Stolper and Newman (1994) allows a trade off between fluid concentrations and the amount of fluid added to MTB sources, even to the point of allowing mixing between hydrous (~4 wt% H_2O) and anhydrous magma or mantle. This ambiguity results in part from the similarity in the order of incompatibility for solid-fluid and solid-melt bulk partition coefficients for highly incompatible elements and also from the fact that, for the highly incompatible elements, hydrous fluids are likely to dominate the trace element and isotopic composition of the melts they engender. Therefore, the distinctive subduction component signature will appear whether it is introduced directly into upwelling BAB mantle or indirectly, through an intermediary arc-like melt.

There are two constraints that we would like to emphasize regarding the nature of the HFA. First, the HFA flux to the MT mimics the arc magma budget. This is demonstrated by the morphological segmentation of the MT axial rift. The MT rift bathymetry, which mimics magma budget and thus the proportion of HFA introduced into the source region, corresponds to variations in magma budget along the Mariana arc. The major subdivision of the arc at latitudes of the SMT is between the high magma budget Central Island Province and the lower magma budget Southern Seamount Province. This boundary occurs at about 16°N (Dixon and Stern, 1983), the same latitude that separates the N-SMT from the S-SMT (Fig. 1). The physical basis for the changes in magmatic budget in the arc and the back-arc basin on either side of 16°N is not understood, but the correspondence in position of the arc and back-arc magma budget boundaries argues for a common explanation. It is possible the boundary corresponds to a major change in the volume of water being released from the slab at depths >100 km but no fundamental differences can be recognized in the composition or thickness of sediments or the age of Western Pacific seafloor subducted at this latitude. Possibly this change in magma budget corresponds to different mantle potential temperatures, with cooler mantle to the south and warmer mantle to the north. There also is apparently a break in the frequency and maximum depth of seismicity at this latitude: north of the break seismic events have occurred as deep as 650+km, whereas south of the break seismicity deeper than 400 km is uncommon (Eguchi, 1984).

The second constraint comes from the observation that the magmatic budget that is generally observed behind arc magmatic fronts and manifested as cross-chain volcanoes (Hussong and Fryer, 1983) is largely missing in the region where seafloor spreading exists in the Mariana Trough. The Izu-Bonin-Mariana arc system is characterized by a large magmatic budget along the magmatic front with decreasing magmatism in volcanoes farther away from the trench (Suga and Fujioka, 1990). The magmatic budget behind the mag-

matic front is manifested as small volcanoes (back-arc knolls of Honza and Tamaki, 1985). The chemical and isotopic composition of the cross-chain volcanoes is distinctively enriched relative to either lavas from the back-arc basin or from the arc magmatic front. Cross-chain volcanoes are abundant in the Izu-Bonin arc where back-arc basin seafloor spreading has not occurred since the Miocene, but are rare behind the Mariana arc. The absence of volcanism behind the Mariana arc magmatic front is consistent with a hypothesis whereby rear arc magmas, or the fluids that cause this, are captured by upwelling mantle beneath the Mariana Trough and so represent the HFA. Alternatively, following the flow regime envisioned by McCulloch and Gamble (1991), this absence may indicate that the enriched mantle otherwise sampled by cross-chain volcanism is depleted during melting to form BAB. In either case, the absence of cross-chains in the Mariana Trough is consistent with the HFA sampling the enriched cross-chain component.

The distinctive isotopic composition of Izu-Bonin-Mariana cross-chain magmas has been noted (Tatsumi et al., 1992; Stern et al., 1993), especially the relatively non-radiogenic Sr at a given Nd. This contrast provides an opportunity to use MTB isotopic data to test the hypothesis that the HFA affecting Mariana Trough basalts is similar to cross-chain melts. Figure 9 shows that the HFA identified by Stolper and Newman (1994) is consistent with the mantle endmember indicated by the SMT data and has less-radiogenic Sr and lower Nd than magmas characteristic of Mariana magmatic front lavas such as the CIP. Mixing trajectories between CIP melts and MORB-type mantle cannot produce hybrids appropriate to SMT or other MTB basalts (Fig. 9, trajectory labeled D84-CIP). The composition of cross-chain lavas, however, is consistent with the mixing trajectories of Stolper and Newman (1994) (compare mixing trajectories labeled Stolper & Newman and D84-Kasuga in Fig. 9).

7. CONCLUSIONS

The SMT has two spreading rift segments, each about 100 km long, that erupt different basalts and so define a new scale of heterogeneity for the Mariana Trough and other back-arc basins. The recovery of true NMORB in the S-SMT confirms the presence of depleted mantle beneath the MT and indicates that the process responsible for basalt generation beneath mid-ocean ridges, adiabatic decompression, also operates beneath back-arc basins. The contrasting magmatic budgets of the N- and S-SMT correlates remarkably well with abundances of highly incompatible elements and water, a result not found for true MORB. These results indicate that flux melting is also critical for the generation of back-arc basin basalts. Questions remain regarding whether the fluxing agent is a hydrous fluid or melt; we prefer the interpretation that it is the arc cross-chain component that is captured by the back-arc convective regime, providing a direct link between magmatically vigorous parts of the Mariana arc and MT and explaining the dearth of rear-arc volcanoes in this region.

Evidence for testing our model must exist south of the only true MORB recovered in the Mariana Trough, located at the southernmost end of the ridge we sampled. How do basalt compositions change as the spreading ridge approaches the Mariana Trench to the south? If the subduction component is transported by a fluid, with no direct relationship to arc magmatism, these basalts should show abundant influence of a slab-derived subduction component. However, because the arc magmatic budget is very low south of 16°N, our model predicts that BABB from the region south of our study area will be similar to MORB. Further work in this region is critical for understanding the generation of these basalts.

Acknowledgments—This research was supported by NSF grants OCE-8918481 and OCE-9302162 to RJS and OCE-8917585 to SHB. We appreciate careful reviews by T. Elliott, R. Hickey-Vargas, and J. Sinton. This is UTD Programs in Geosciences Contribution #823.

Editorial handling: J. D. Morris

REFERENCES

Barone A. M., Lonsdale P. F., and Puteanus D. (1990) Formation of axial ridges of the Mariana slow spreading center from spaced magma sources. *EOS* **71,** 1637–1638.

Bibee L. D., Shor G. G., Jr., and Lu R. S. (1980) Inter-arc spreading in the Mariana Trough. *Mar. Geol.* **35,** 183–197.

Chow T. J., Stern R. J., and Dixon T. H. (1980) Absolute and relative abundances of K, Rb, Sr, and Ba in Circum-Pacific Island-Arc magmas, with special reference to the Marianas. *Chem. Geol.* **28,** 111–121.

Davies J. H. and Bickle M. J. (1991) A physical model for the volume and composition of melt produced by hydrous fluxing above subduction zones. *Phil. Trans. Roy. Soc. London* **335,** 355–364.

Davies J. H. and Stevenson D. J. (1992) Physical Model of Source Region of Subduction Zone Volcanics. *J. Geophys. Res.* **97,** 2037–2070.

Delaney J. R., Muenow D. W., and Graham D. G. (1978) Abundance and distribution of water, carbon, and sulfur in the glassy rims of submarine pillow basalts. *Geochim. Cosmochim. Acta* **42,** 581–594.

Dixon T. H. and Stern R. J. (1983) Petrology, chemistry, and isotopic composition of submarine volcanoes in the southern Mariana arc. *Geol. Soc. Amer. Bull.* **94,** 1159–1172.

Dixon, J. E., Stolper E. M., and Delaney J. R. (1988) Infrared spectroscopic measurement of CO_2 and H_2O in Juan de Fuca Ridge basaltic glasses. *Earth Planet. Sci. Lett.* **90,** 97–104.

Eguchi T. (1984) Seismotectonics around the Mariana Trough. *Tectonophysics* **102,** 33–52.

Fryer P. (1995) Geology of the Mariana Trough. In *Backarc Basins: Tectonics and Magmatism* (ed. B. Taylor), pp. 237–279. Plenum Press.

Fryer P., Sinton J. M., and Philpotts J. A. (1981) Basaltic glasses from the Mariana Trough. *Initial Rep. Deep Sea Drill. Proj.* **60,** 601–609.

Garcia M. O., Liu N. W. K., and Muenow D. W. (1979) Volatiles in submarine volcanic rocks from the Mariana Island arc and trough. *Geochim. Cosmochim. Acta* **43,** 305–312.

Hart S. R. (1984) A large-scale isotope anomaly in the southern hemisphere mantle. *Nature* **309,** 753–757.

Hart S. R. (1988) Heterogensous mantle domains: Signatures, genesis and mixing chronologies. *Earth Planet. Sci. Lett.* **90,** 273–296.

Hart S. R., Glassley W. E., and Karig D. E. (1972) Basalts and sea floor spreading behind the Mariana Island Arc. *Earth Planet. Sci. Lett.* **15,** 12–18.

Hawkins J. W. and Melchior J. T. (1985) Petrology of Mariana Trough and Lau Basin basalts. *J. Geophys. Res.* **90,** 11,431–11,468.

Hawkins J. W., Macdougall J. D., and Volpe A. M. (1990) Petrology

of the axial ridge of the Mariana Trough backarc spreading center. *Earth Planet. Sci. Lett.* **100,** 226–250.

Hickey-Vargas R. (1991) Isotope characteristics of submarine lavas from the Philippine Sea: Implications for the origin of arc and basin magmas of the Philippine tectonic plate. *Earth Planet. Sci. Lett.* **107,** 290–304.

Hickey-Vargas R., Hergt J. M., and Spadea P. (1995) The Indian Ocean-type isotopic signature in western Pacific marginal basins: origin and significance. In *Active Margins and Marginal Basins of the Western Pacific* (ed. B. Taylor and J. Natland); *AGU Geophys. Monogr.* **88,** 175–197.

Hole M. J., Saunders A. D., Marriner G. F., and Tarney J. (1984) Subduction of pelagic sediments: Implications for the origin of Ce-anomalous basalts from the Mariana Islands. *J. Geol. Soc. London* **141,** 453–472.

Hofmann A. W. (1988) Chemical differentiation of the Earth: The relationship between mantle, continental crust, and oceanic crust. *Earth Planet. Sci. Lett.* **90,** 297–314.

Honza E. and Tamaki K. (1985) The Bonin Arc. In *The Ocean Basins and Margins* (ed. A. E. M. Nairn et al.), pp. 459–502. Plenum.

Hussong D. M. and Fryer P. (1983) Back-arc seamounts and the SeaMARC II seafloor mapping system. *EOS* **64,** 627–632.

Hussong D. M. and Uyeda S. (1981) Tectonic processes and the history of the Mariana Arc: A synthesis of the results of Deep Sea Drilling Project leg 60. *Initial Rep. Deep Sea Drill. Proj.* **60,** 909–929.

Karig D. E. (1971) Origin and development of marginal basins in the western Pacific. *J. Geophys. Res.* **76,** 2542–2561.

Kinzler R. J. and Grove T. L. (1992) Primary magmas of Mid-Ocean Ridge Basalts 2. Applications. *J. Geophys. Res.* **97,** 6907–6926.

Klein E. M. and Langmuir C. H. (1987) Global correlations of ocean ridge basalt chemistry with axial depth and crustal thickness. *J. Geophys. Res.* **92,** 8089–8115.

Kress V. C. and Carmichael I. S. E. (1988) Stoichiometry of the iron oxidation reaction in silicate melts. *Amer. Mineral.* **73,** 1267–1274.

Lin P.-N., Stern R. J., Morris J., and Bloomer S. H. (1990) Nd- and Sr-isotopic composition of lavas from the northern Mariana and southern Volcano arcs: Implications for the origin of island arc melts. *Contrib. Mineral. Petrol.* **105,** 381–392.

Mahoney J., leRoex A. P., Peng Z., Fisher R. L., and Natland J. H. (1992) Southwestern limits of Indian Ocean ridge mantle and the origin of low $^{206}Pb/^{204}Pb$ mid-ocean ridge basalt: Isotope systematics of the central Southwest Indian ridge. *J. Geophys. Res.* **97,** 19,771–19,790.

Mahoney J. J., Sinton J. M., Kurz M. D., Macdougall J. D., Spencer K. J., and Lugmair G. W. (1994) Isotope and trace element characteristics of a super-fast spreading ridge: East Pacific rise, 13–23°S. *Earth Planet. Sci. Lett.* **121,** 173–193.

Malinverno A. (1993) Transition between a valley and a high at the axis of mid-ocean ridges. *Geology* **21,** 639–642.

Manton W. I. (1988) Separation of Pb from young zircons by single-bead ion exchange. *Chem. Geol.* **73,** 147–152.

Martinez F., Fryer P., Baker N. A., and Yamazaki T. (1995) Evolution of Backarc Rifting: Mariana Trough, 20°–24°N. *J. Geophys. Res.* **100,** 3807–3827.

McCulloch M. T. and Gamble J. A. (1991) Geochemical and geodynamical constraints on subduction zone magmatism. *Earth Planet. Sci. Lett.* **102,** 358–374.

Meijer (1976) Pb and Sr isotopic data bearing on the origin of volcanic rocks from the Mariana island-arc system. *Geol. Soc. Amer. Bull.* **87,** 1358–1369.

Melson W. G., Vallier T. L., Wright T. L., Byerly G., and Nelen J. (1976) Chemical diversity of abyssal volcanic glasses erupted along Pacific, Atlantic and Indian ocean sea-floor spreading centers. In *The Geophysics of the Pacific Ocean Basin and its Margin* (ed. G. H. Sutton et al.); *AGU Geophys. Monograph* **19,** 351–367.

Michael P. J. (1988) The concentration, behavior, and storage of H_2O in the suboceanic upper mantle: Implications for mantle metasomatism. *Geochim. Cosmochim. Acta* **52,** 555–566.

Muenow D. W., Garcia M. O., Aggrey K. E., Bednarz U., and Schmincke H. U. (1990) Volatiles in submarine glasses as a discriminant of tectonic origin: Application to the Troodos ophiolite. *Nature* **343,** 159–161.

Park C., Tamaki K., and Kobayashi K. (1990) Age-depth correlation of the Philippine Sea back-arc basins and other marginal basins in the world. *Tectonophysics* **181,** 351–371.

Pearce J. A. and Peate D. W. (1995) Tectonic implications of the composition of Volcanic Arc Magmas. *Ann. Rev. Earth Planet. Sci.* **23,** 251–285.

Pier J. G., Podosek F. A., Luhr J. F., Brannon J. C., and Aranda-Gomez J. J. (1989) Spinel-lherzolite-bearing Quaternary volcanic centers in San Luis Potosi, Mexico. 2. Sr and Nd isotopic systematics. *J. Geophys. Res.* **94,** 7941–7951.

Richard P., Shimizu N., and Allègre C. J. (1976) $^{143}Nd/^{146}Nd$, a natural tracer. An Application to oceanic basalts. *Earth Planet. Sci. Lett.* **31,** 269–278.

Saunders A. D., Norry M. J., and Tarney J. (1991) Fluid influence on the trace element compositions of subduction zone magmas. *Phil. Trans. Roy. Soc. London A* **335,** 377–392.

Sinton J. M. and Fryer P. (1987) Mariana Trough lavas from 18°N: Implications for the origin of back arc basin basalts. *J. Geophys. Res.* **92,** 12,782–12,802.

Sisson T. W. and Grove T. L. (1993) Experimental investigations of the role of H_2O in calc-alkaline differentiation and subduction zone magmatism. *Contrib. Mineral. Petrol.* **113,** 143–166.

Solomon S. C. and Toomey D. R. (1992) The structure of mid-ocean ridges. *Annu. Rev. Earth Planet. Sci.* **20,** 329–364.

Stern R. J., Lin P., Morris J. D., Jackson M. C., Fryer P., Bloomer S. H., and Ito E. (1990) Enriched back-arc basin basalts from the northern Mariana Trough: Implications for the magmatic evolution of back-arc basins. *Earth Planet. Sci. Lett.* **100,** 210–225.

Stern R. J., Jackson M. C., Fryer P., and Ito E. (1993) O, Sr, Nd, and Pb isotopic composition of the Kasuga Cross-Chain in the Mariana Arc: A new perspective on the K-h relationship. *Earth Planet. Sci. Lett.* **119,** 459–475.

Stolper E. and Newman S. (1994) The role of water in the petrogenesis of Mariana Trough magmas. *Earth Planet. Sci. Lett.* **121,** 293–325.

Suga J. and Fujioka K. (1990) Volume of volcanic materials along Northern Izu-Bonin arc. *Bull. Vol. Soc. Japan* **2-35,** 359–374.

Sun S.-S. and McDonough W. F. (1989) Chemical and isotopic systematics of oceanic basalts: Implications for mantle composition and processes. In *Magmatism in the Ocean Basins* (ed. A. D. Saunders and M. J. Norry); *Geol. Soc. Spec. Publ.* **42,** 313–345.

Tatsumi Y., Hamilton D. L., and Nesbitt R. W. (1986) Chemical characteristics of fluid phase released from a subducted lithosphere and origin of ore magmas: Evidence from high-pressure experiments and natural rocks. *J. Volcan. Geotherm. Res.* **29,** 293–309.

Tatsumi Y., Murasaki M., and Nohda S. (1992) Across-arc variation of lava chemistry in the Izu-Bonin Arc: Identification of subduction components. *J. Volc. Geotherm. Res.* **49,** 179–190.

Thompson A. B. (1992) Water in the Earth's upper mantle. *Nature* **358,** 295–302.

Tormey D. R., Grove T. L., and Bryan W. B. (1987) Experimental petrology of normal MORB near the Kane Fracture Zone: 22°–25°N, mid-Atlantic ridge. *Contrib. Mineral. Petrol.* **96,** 121–139.

Volpe A. M., Macdougall J. D., and Hawkins J. W. (1987) Mariana Trough basalts (MTB): Trace element and Sr-Nd isotopic evidence for mixing between MORB-like and arc-like melts. *Earth Planet. Sci. Lett.* **82,** 241–254.

Volpe A. M., Macdougall J. D., Lugmair G. W., Hawkins J. W., and Lonsdale P. (1990) Fine-scale isotopic variation in Mariana Trough basalts: Evidence for heterogeneity and a recycled component in backarc basin mantle. *Earth Planet. Sci. Lett.* **100,** 251–264.

Woodhead J. D. and Fraser D. G. (1985) Pb, Sr, and ^{10}Be isotopic studies of volcanic rocks from the Northern Mariana Islands. Implications for magma genesis and crustal recycling in the Western Pacific. *Geochim. Cosmochim. Acta* **49,** 1925–1930.